Substorm entropies

Simon Wing[1] and Jay R. Johnson[2]

[1]The Johns Hopkins University Applied Physics Laboratory, Laurel, Maryland, USA

[2]Princeton Plasma Physics Laboratory, Princeton, New Jersey, USA

Abstract. The specific entropies ($s = p/n^{\gamma}$) and total entropies ($S= p^{1/\gamma}V$) of the plasma sheet during substorm are investigated with DMSP observations using a method that assumes ion isotropy, as assumed in the derivation of $p^{1/\gamma}V$. During quasi-steady periods, i.e. growth phase, (a) S and flux tube contents (N) decrease with decreasing distance from the Earth, commonly known as pressure balance inconsistency; (b) s appears to be conserved in the X or convection direction; and (c) there is a dawn-dusk heat flux consistent with curvature/gradient drift. In the early and late recovery phases, s has a minimum at postmidnight that can be associated with cold dense ions. During the phase transitions, S is reduced by an order of magnitude earthward of 20 Re. This result is consistent with a recent MHD simulation that shows that after reconnection S is reduced with the difference residing in the plasmoid that forms tailward of the X line. Interestingly, s does not change before and after reconnection, suggesting that reconnection only affects the small dissipation region, leaving most of the plasma unchanged and conserving s of the system.

1. Introduction

The substorm is one of the most interesting and complex phenomena in space physics. Its development has generally been categorized into three phases: growth, expansion, and recovery. The growth phase is typically defined as the quiescent period starting at the time of the southward turning of the Interplanetary Magnetic Field (IMF) and ending at the onset of the expansion phase (commonly referred to as the substorm onset). During growth phase, the auroral oval expands equatorward, the aurora and the electrojet gradually intensify, the plasma sheet thins, and the magnetospheric magnetic field lines stretch (become tail-like), as the solar wind energy is stored in the magnetotail. The growth phase is followed by the expansion phase, during which the auroral oval expands poleward, eastward, and westward, and the magnetic field configuration in the inner plasma sheet changes rapidly from the stretched tail-like configuration to a more dipolar configuration. The expansion phase is followed by the recovery phase, which corresponds to the return of the magnetosphere to the undisturbed state. A more detailed description of substorm phases can be found in *Lui* [1991].

In considering the dynamics of substorms [not necessarily the trigger(s)], it is useful to identify conserved quantities, which place constraints on dynamical evolution. Although conserved quantities help simplify the description of the dynamics when they apply, it is often useful to identify where and when the conservation law is broken because it typically requires a more complex description of the dynamics.

One fundamental conserved quantity is the entropy, which is conserved when the plasma response is adiabatic. In the ideal MHD description, the pressure response is generally prescribed as adiabatic such that the entropy per unit mass (also referred to as specific entropy), $s= p/\rho^{\gamma}$, is constant for a fluid element where p = the plasma pressure, B = magnetic field, γ = the polytropic index. The specific entropy, s, should be rigorously conserved in an ideal MHD fluid

element and is an intensive variable in that it does not depend on system size. The pressure equation also implies an integral constraint on the total mass content of a flux tube, $M = \int \rho\, ds/B$ which is proportional to $S = \int p^{1/\gamma}\, ds/B$. Although not precisely the entropy of the flux tube, this quantity S is entropy-like in nature [*Birn et al*., 2006a] and we will refer to it as the total entropy. The total entropy is also an important parameter to identify when the interchange instability is operable.

Nonconservation of specific entropy is expected to occur when nonadiabatic processes such as wave-particle interactions, heat flux, and dissipation are operating and when the fluid element looses its integrity as occurs when hot particles and cold particles move differently (e.g. cold particles move with ExB convection and hot particles move by curvature and gradient drift). Nonconservation of the total entropy can occur under these same conditions and is generally associated with the loss of plasma content from a flux tube.

Several statistical studies have examined the properties of the specific and total entropy in the plasma sheet. In the case of a single ion species, $p/\rho^{\gamma} \sim p/n^{\gamma}$. If s is conserved along the convection path, then, in the p – n space, plasma sheet ion p and n should follow lines having constant slopes of γ, termed adiabats. Borovsky et al. [1998] shows that statistically this seems to be the case from midtail region (X = -22.5 Re) to geosynchronous orbit (X = - 6.6 Re) in their p – n plots (see their Plate 1). Borovsky et al. [1998] finds that $\gamma = 1.52$, which is close to 5/3, albeit the scatters are quite large. Similar result has been obtained by Baumjohann [1993] that reports that $\gamma \sim 1.69$ also with large scatters in its p – n plots.

On the other hand, statistical studies have shown fairly definitively that in the magnetotail, S is not conserved — S decreases with decreasing distance from Earth. Erickson and Wolf [1980] first notes this phenomenon and names it pressure balance inconsistency (which lately has been termed pressure crisis perhaps because since its formulation almost two decades

ago, it remains a challenge to the contemporary space physics). As formulated by Erickson and Wolf [1980], if the flux tube is in pressure balance at distant tail, X ~ -60 Re, and the flux tube convects earthward adiabatically (S is conserved), by the time it reaches the inner plasma sheet, X ~ -10 Re, the pressure would be too high to maintain pressure balance with a typical average magnetic field obtained from observations or an empirically based time independent magnetic field model. Erickson and Wolf [1980] speculates that substorm process somehow nonadiabatically ejects plasma tailward, reducing the pressure at the inner plasma sheet. Recently, Birn et al. [2006a] simulates substorm where following near-Earth reconnection, plasmoid formation in the tail leads to a decrease of S on the field lines attached to Earth. In other words, S is reduced by shedding the field line and entropy carried by the tailward travelling plasmoid. Other mechanisms to resolve the pressure balance inconsistency have been proposed such as gradient/curavature drift [Tsyganenko, 1982; Kivelson and Spence, 1988; Wang et al. [2001], non earthward ExB drift [e.g., Kaufmann, 2004], plasma bubbles or bursty bulk flows [e.g., Pontius and Wolf,1990; Chen and Wolf, 1993]).

In the present paper, we will examine how the ion transport modifies or conserves s and S in the plasma sheet during active time (substorm). The total entropy S is a global property that cannot be obtained from local measurements while s can be obtained from local observations. Furthermore, an increase or reduction in S does not necessarily mean a change in s [e.g., Birn et al., 2004;2006; Wing et al.,2007].

For purposes of this study, because the plasma sheet electron contribution to the total pressure is much smaller, roughly 15% [e.g., Baumjohann et al., 1989; Spence et al., 1989], than the ion pressure, it is possible to probe the plasma sheet entropy considering only ion data. In the plasma sheet, ions have been observed to be nearly isotropic irrespective of magnetic activities [Kistler et al., 1992; Huang and Frank, 1994; Spence et al., 1989] due to strong (elastic) pitch

angle scattering [e.g., Lyons and Speiser, 1982] and long drift time compared to the bounce period [e.g., Wolf, 1983]. Fortunately, the isotropy of the ions makes it possible to remotely probe the ion distributions by observing only precipitating particles in the ionosphere, as discussed later. Moreover, because the pressure is observed to be isotropic, the total entropy can be simplified when the system is near equilibrium because the pressure is constant along field lines and $S=\int p^{1/\gamma}\, ds/B \sim p^{1/\gamma}V$ (V is flux tube volume) is conserved. Interestingly, Usadi et al. [2006] notes that even when the particle motion violates both first and second adiabatic invariant, S is still conserved. The value for γ can range from 0 to ∞, depending on the process(es) involved. For example, for isobaric (constant pressure) system $\gamma = 0$; for isothermal (constant temperature) system $\gamma = 1$; for isometric (constant density) system $\gamma = \infty$; and for adiabatic (no heat loss) system and monoatomic gas $\gamma = 5/3$. $S = p^{1/\gamma}V$ is an extensive parameter that is proportional to system size, e.g., flux tube volume V.

In the remainder of this paper, section 2 briefly discusses our substorm selection criteria; section 3 explains our technique to estimate the entropy of the plasma sheet using ionospheric data from DMSP; section 4 presents substorm entropy profiles; section 5 discusses the implications of our study for understanding substorm dynamics; and section 6 summarizes our findings.

2. Substorm event selections

Wing et al. [2007] examines S and s near midnight meridian and finds that in the near-Earth region, S decreases dramatically after substorm onset while interestingly, s remains roughly conserved. The present study extends Wing et al. [2007] study to the entire plasma sheet region in the equatorial plane.

The substorm events were selected using criteria described in Wing et al. [2007] and Gjerloev et al. [2007]. Care has to be given to make sure that the substorm events are isolated and not concurrent with other types of disturbances such as the shock or pressure pulse. In all, a total of 180 substorm events were selected for the present study.

The substorm phases were normalized by the onset of brightening (T_0) and the peak of the substorm (T_1). The selection of these times was based purely on the global auroral images. Utilizing both the Polar VIS Earth Camera and the Polar UVI enables us to determine the onset time to within 1 min, which is sufficiently accurate for the present study. The substorm maximum or end of the expansion phase (T_1) is based on a qualitative estimate of the time at which the combined optical emission intensity and the poleward expansion of the aurora are or near maximum. The intensity often begins to fade before the expansion ceases, especially at the end of the bulge [*Gjerloev et al*., 2007]. Thus the selection of the global aurora maximum or peak incorporates optical characteristics. In agreement with the more classical definition of the peak, *Gjerloev et al.* [2007] shows that this technique results in the maximum substorm time that coincides with the average minimum AL. The duration of the expansion phase is defined as $\Delta t = T_1 - T_0$. Δt ranges from 7 to 92 min with a median of 32 min and a mean of 35 ± 18 min. The four phases analyzed in this study are:

- (onset – Δt) ≤ growth phase < onset.
- onset ≤ expansion phase < (onset + Δt)
- (onset + Δt) ≤ early recovery phase < (onset + $2\Delta t$)
- (onset + $2\Delta t$) ≤ late recovery phase < (onset + $3\Delta t$)

3. Data and methodology

The DMSP SSJ4 instrument measures only highly field-aligned precipitating particles at energy range of 32 eV to 30 keV at an altitude of roughly 835 km. Plasma sheet ions have been observed to be nearly isotropic irrespective of the activity levels [e. g., *Kistler et al*., 1992]. Taking advantage of these properties, *Wing and Newell* [1998; 2000; 2002] has developed a method for inferring the plasma sheet ion temperature, density, and pressure from the DMSP SSJ4 measurements. The present study uses essentially the same method, which has been fully described in *Wing and Newell* [1998], with the following modifications deemed necessary for substorm studies.

As noted in section 1, the topology of the magnetospheric magnetic field changes rapidly during the evolution of the substorm loading-unloading cycle. This complicates the ionosphere-plasma sheet mapping. Instead of using the real values of b2i and Kp as inputs to the modified T89 magnetic field model [*Tsyganenko*, 1989], as done by *Wing and Newell* [1998], we utilized the original unmodified T89 with the following caveat. The Kp input to the T89 was fixed to 4, 1, 2, and 2 for growth, expansion, early recovery, and late recovery phases, respectively. We believe that the resulting T89 magnetic field line would more closely resemble the well-known magnetic field configurations during these substorm phases. *Opgenoorth et al*. [1994] compares the disturbed-time ionosphere-to-equatorial plane mapping of the original T89, which does not have field-aligned currents (FAC), with that of T89 + FAC. The study finds that the two methods result in locations that differ by a few R_E in the equatorial plane (Figure 6 of *Opgenoorth et al*. [1994]). *Pulkkinen and Tsyganenko* [1996] also evaluates the ionosphere-to-equatorial plane mapping in T89, which is symmetrical with respect to midnight meridian, and finds the errors for points originating in the auroral oval to be within a few R_E in the X or Y direction (see also *Wolf et al*. [2006] for evaluating entropy with T89). In light of these estimated mapping uncertainties and the limited number of events, we averaged the pressures,

densities, and temperatures in 3 × 3 R_E^2 bins. The difficulty of accurate ionosphere-magnetosphere mapping is certainly a concern in the present study, which limits the results to only the large-scale spatiotemporal behavior of the fundamental plasma sheet parameters.

Another important aspect of this method is that instead of computing moments, which is commonly done, each ion spectrum is fitted to distribution functions (one-component Maxwellian, two-component Maxwellian, and κ), and the best fit is selected. This takes into account ions outside the detectors' energy range. Therefore, the densities obtained can be larger than those calculated using moments. Moments may also underestimate temperatures by ignoring the hotter components (when they are significant), which may explain some of the temperature differences resulting from using the two methods. Electron acceleration (inverted V) events, which usually indicate the presence of significant field-aligned electric field, were eliminated from our database.

Five DMSP satellites were operational in the 1997-2001 interval, F10, F11, F12, F13, and F14. Out of the 180 substorm events, 132 events have simultaneous DMSP particle observations. Figure 1 shows an example from October 23, 1997 event. The top row displays the Polar VIS Earth Camera images obtained during the four above-defined substorm phases. The DMSP passes are superposed onto the Polar VIS images, showing the locations of the ion data used to infer the equatorial plasma sheet pressure shown at the bottom row.

4. Substorm entropy profiles

4.1. Quasi-steady entropy profiles

During periods of quasi-steady magnetospheric behavior without significant nonadiabatic processes, such as particle heating or diffusion, it may be expected that plasma evolves in some regions with near-laminar motion (or at least particles in a certain energy range evolve with near

laminar motion). Under these conditions (assuming steady plasma sources), it would be expected that the total entropy and specific entropy both would be conserved along streamlines (particle trajectories for a given energy range) and isoentropy contours would be an indicator of drift paths. We consider the behavior of S and s during the substorm phases assuming quasi-steady magnetospheric behavior has been reached.

The pressure, temperature, and density profiles for substorm phases are shown in Figure 1 [from Figure 2 of Wing et al., 2007]. S ($p^{1/\gamma}V$) and s (p/ρ^{γ}) in the equatorial plane can be calculated from these profiles. Figure 2 panels a – d (the left panels) show s for growth, expansion, early recovery, and late recovery periods respectively while panels e – h (the right panels) show the same for S.

During the growth phase, e.g., steady state convection, Figure 2e shows that S decreases with decreasing radial distance from the Earth. This result is qualitatively similar to the statistical result obtained by Garner et al. [2003] (see their Figure 4). This phenomenon has been previously reported as the pressure balance inconsistency or pressure crisis [e. g., Erickson and Wolf, 1980; Erickson, 1992; Garner et al., 2003; Kaufmann et al., 2004]. In contrast to the total entropy, S, Figure 2a shows also that isocontours of specific entropy, s, tend to align in the X direction suggestive that earthward convection could be organizing the plasma profiles in the tail. However, Figure 2a also shows that there is a dawn-dusk asymmetry in the s profile with the duskside having higher entropy than the dawnside, which is more pronounced closer to Earth. This asymmetry would be consistent with the duskward heat flux carried by the curvature and gradient B drift which is in the duskward direction for ions and typically becomes more dominant than earthward convection due to a dawn-dusk convection electric field closer to the earth.

An interesting feature in the early and late recovery profiles is that there is an s minimum at postmidnight at the inner edge of the plasma sheet as shown in Figure 2c and 2d. This entropy reduction is associated with the cold dense ions found in this region that as shown in Figure 1 panels g, k, h, and l. These cold dense ions appear confined to a small region at the inner edge of the plasma sheet in the early recovery phase, but spread tailward in the late recovery phase. The origin of these cold dense ions is not clear, but studies have shown that the ion outflow rate peaks about 20 to 30 min after substorm onset and remains at an elevated level up to 70 min or even beyond 90 min, depending on the methodology [e.g., *Wilson et al*., 2004; Tung et al., 2001]. In the plasma sheet, the ion outflow would arrive first at the inner edge of the plasma sheet and spread tailward because of the time of flight effect, consistent with the observations. Assuming that the average energy of 1 keV and direct paths from nightside ionosphere, O+ will arrive in the equatorial plane at 10 Re at about 14 min and at 30 Re at about x min. Of course, in the plasma sheet, the ionospheric ions are mixed with the plasma sheet ions and hence the mean ion temperatures are higher than ionospheric temperatures but lower than plasma sheet temperatures. It is expected that the effect of the ion outflow in the plasma sheet is cumulative such that the number of ionospheric ions continuously increases in the immediate aftermath of the onset. The loading of cold material onto magnetospheric field lines can also increase the mass content and S. Typically S increases tailward, however, if enough material were loaded locally onto a flux tube the S profile could be expected to decrease tailward of that flux tube leading to the possibility of interchange. However, statistically this was not observed in the present study. Figure 2 panels c and d show that S increases tailward. This perhaps suggests that the cold ions may not contribute significantly to the pressure, but it needs to be investigated further.

4.2. Phase Transitions and Entropy Profiles

At the substorm onset, there is a large-scale dynamic transition in the magnetospheric state as energy stored in the tail is released and the magnetic field dipolarizes. To gain insight regarding the dynamic process leading to the new state, we consider entropy prior to and after substorm onset. Nonconservation of entropy results from nonadiabatic processes, e.g., turbulent transport, thermal energy transport due to nonadiabatic particle drifts, or precipitation, and may indicate which processes are most important in the transition to the new state of the system. Although such comparisons may not necessarily identify a substorm trigger, they do raise some important issues.

To compare the entropy change in the transition from the growth phase to the expansion phase, we consider the flux tube volumes for field lines that share the same footpoint (point B) as shown in Figure 3. In doing so, we ignore the slow slippage of the footpoints on a convective timescale. Using T89, point B is traced along the field line for Kp = 4 (growth phase; more stretched field lines) and Kp = 1 (expansion phase; more dipolarized field lines) to points A and C, respectively, on the equatorial plane (minimum |**B**|), as sketched in Figure 3. Wing et al. [2007] compares the entropy at these two different locations in the midnight meridian: at midtail region (A = –30 R_E, C = –20 R_E) and at near-Earth region (A = –20 R_E, C = –7 R_E) and finds that after onset, S decreases by a factor of 8 in the depolarized region near the Earth, but S slightly increases at the midtail region as tabulated in Table 1 (from Wing et al., [2007]). Interestingly, s does not appear to change much after onset for the field lines in the midnight meridian.

The present study expands the Wing et al. [2007] study by comparing changes in S and s between the growth, expansion, and recovery phases over the entire 2D equatorial plane. The results are shown in Figure 4. Panel 4a shows $\log_{10}$(Se/Sg) where Se = S expansion phase and

Sg = S growth phase. The panel shows that in the region earthward of 20 Re between |Y| < 10 Re, S is reduced by an order of magnitude, log10(Se/Sg) ~ -1, consistent to the midnight profile shown in Table 1. In contrast, as shown in panel 4a, s appears to remain roughly the same after onset. We have also compared s from early and late recovery phases to those from growth phase, as shown in Figure 4 panels b and c respectively. These panels again reinforce the notion that s does not appear to change much throughout the substorm phases. In the recovery phase, the plasma state appears to be moving closer to the growth phase state. Figure 4 panels e and f compare Ser = S early recovery phase and Slr = S late recovery phase to the Sg, respectively. In the region earthward of 20 Re and |Y| < 10 Re, log10 (Ser/Sg) and log10(Slr/Sg) are still negative, indicating that the early and late recovery phases, Ser and Slr, are still at a reduced level compared to growth phase Sg. However, Sr appears to be closer to Sg than Se to Sg, as evidenced by the lighter blue color in panels e and f than in panel d. Moreover, in the region tailward of 20 Re, the region which has similar S as in the growth phase (whitish region in Figure 4d) has expanded.

It should be noted that several assumptions are made in this comparison. First, in order to compute S, we assume that a particular flux tube is in quasi-steady equilibrium. We also assume that the pressure is isotropic, which is at least more or less consistent with observations and our mapping technique. With that assumption, we can compute $S = p^{1/\gamma} V$. However, the flux tube volume is computed from the Tsganenko field, which is not really in equilibrium, but it is at least consistent with our mapping technique. Given that we are computing profiles for a statistical ensemble of magnetospheric configurations anyway, the errors involved are probably secondary to the question of whether there is a quasi-steady equilibrium. To consider the statistical ensemble of measurements taken on a flux tube during the entire expansion period to be useful, that flux tube should be in a quasi-steady equilibrium state during most of the expansion period.

From the MHD perspective, the simulations of Birn et al. [2006a] suggest that once a field-line has reconnected that it behaves as if it were a slowly varying equilibrium field. Proceeding with the assumption that S is conserved and MHD is valid, it is therefore useful to consider the total entropy on field lines that reconnect early in the expansion phase. Field lines that reconnect later in the expansion phase will (1) not map properly and (2) provide two different values of S depending on whether it is early or late expansion phase. We therefore add the proviso that only the "near earth" mapping results for the expansion phase are meaningful. As S is typically reduced during the substorm it would be expected that the statistical average more likely overestimates the value of S in the expansion phase. The important point is that the near-earth mapping field lines do show a loss of entropy by a factor of about 10 relative to the growth phase value, i.e. most of the plasma has been lost from those flux tubes.

5. Discussion

As discussed in Section 4, S is reduced by about an order of magnitude after substorm onset, as shown in Figure 4d. The entropy reduction after onset is consistent with previous Geotail observations [e.g., *Wolf et al*., 2006]. It has been attributed to the combined effect of the plasma pressure (and density) decrease and dipolarization in the near-Earth region [e.g., *Lyons et al*., 2003a]. Entropy reduction is also found in the simulation of *Birn et al.* [2006a], where plasmoid formation in the tail leads to a decrease of S on field lines attached to Earth following reconnection (essentially by shedding the entropy carried in the plasmoid). The MHD and PIC simulations performed by Birn et al. [2006a] suggest that the dissipation region in reconnection simulations is small (s is conserved away from the dissipation region) and hardly affects the total entropy which is an integral constraint over an entire flux. Consequently, for a closed system the total entropy, S, is essentially conserved, but for the magnetotail simulation, conservation of S

means that the total entropy (of the field connected to earth and the plasmoid) would be conserved. Additionally, total entropy of the flux tube attached to earth and the total entropy of the plasma are each individually conserved following the topological change caused by reconnection. To illustrate, we consider the evolution of the field line and entropy during the substorm is depicted in Figure 5 (from Figures 2 and 3 in Birn et al. [2006a]). The left panels show the magnetic field line configuration in the X - Z plane as a function of time, from t = 0 to t = 100 (each field line is a constant value of vector potential, A, shown in the right panels). For the discussion herein, it is illustrative to follow the evolution of the field line colored in red (at a fixed value of A as indicated by the dashed red line in panel b) as it evolves. We will also follow the entropy evolution of the system, which is given in panel b. Panel b tracks the evolution of the entropy at t = 0, t = 50, t = 70, and t = 100, corresponding to Figure 5a panels from top to bottom. Here, it suffices to focus only at t = 0 (yellow), t = 50 (green), and t = 100 (blue). Initially, at t = 0, the field line is stretched, e.g., the growth phase and its entropy is given by the intersection of the dashed red and yellow lines in plot 5b. At t = 50, the field line stretches around the ejected plasmoid from an earlier reconnection, resulting in a slight increase of S (intersection of dashed red and green lines) in panel b. Reconnection occurs between t = 50 and t = 70. After reconnection, the stretched field line depolarizes and sheds field line which forms plasmoid tailward of the X line. This can be seen at the bottom most panel for t = 100, which shows that the red field line now has splintered into two: one that is still attached to the Earth (closed field line) and the other which forms the red plasmoid. In panel b, we can see that S of the field line that is still attached to the Earth at t = 100 (intersection of the dashed red and blue lines) is much reduced from its original value at t = 0 or t = 50 with the difference is now residing in the plasmoid (not shown). The entropy is reduced because of a topological change in the flux tube volume. Once the field line has reconnected, it is clear that the value of S is

conserved because it remains at the same value at later stages of the simulation. Interestingly, subsequent field-lines that reconnect also reduce to basically the same value of S even though their initial S was significantly different. Because of this conservation of S after reconnection, it is possible to consider the statistical ensemble average over the expansion phase of near-earth field-lines that have reconnected early in the expansion phase to obtain a meaningful comparison with growth phase entropies.

The fact that s remains roughly (but not exactly) conserved after substorm onset is suggestive that whatever process is responsible for the reduction in S is leading to mass loss without significant dissipation. The simulations of Birn et al., [2006b] were performed to investigate how the entropy changes on magnetic field lines during the reconnection process (Harris type current sheet). Both resistive 2D MHD and PIC simulations were performed. It was found that s was conserved except in the dissipation region and therefore S was conserved in either the MHD or PIC simulations. Hence, reconnection does not alter the entropy except in the diffusion region, which is very small. Simply stated, the fact that a field line reconnects does not change the local plasma properties along most of the field line, but it does change its connectivity and therefore the length of the field line (which can alter S).

It is also of interest to consider the relevance of our results on the convection model within each phase of the substorm. The growth phase might be expected to exhibit a steady-state convection. When comparing the entropy at two locations during the growth phase (–30 and –20 R_E), a decrease of S by a factor of 1.5 is found. This is to be contrasted with the decrease of S by a factor of 8 – 10 in the transition from growth phase to expansion phase. This result suggests that there may be a decrease of S during the growth phase, consistent with the finding of *Goertz and Baumjohann* [1991]. This phenomenon is known as the pressure balance inconsistency or pressure crisis [e. g., Erickson and Wolf, 1980; Erickson, 1992; Garner et al., 2003; Kaufmann et

al., 2004]. The decrease of S by a factor of 1.5 from X = -30 Re to X = -20 Re, i.e., a reduction of 1/1.5 or 67%, is consistent with Kaufmann et al. [2004] statistical study with Geotail data that suggests that the average earthward convection losses S by about 15% for every 2.5 Re.

Over the years, a number of studies have suggested several different mechanisms that can relieve the pressure at the inner edge of the plasma sheet and hence explain the pressure inconsistency problem. Pontius and Wolf [1990] suggests that bubbles of underpopulated flux tubes in the plasma sheet would help to resolve the pressure balance inconsistency through differential drift of flux tubes. The bubbles or flux tubes with smaller pressure and density would drift earthward of the adjacent flux tubes with higher pressure and density, resulting in net reduction of S compared to the adjacent flux tubes. However, observations of BBFs (a kind of bubble) show that the average pressure inside the high-speed bursts is slightly higher than in the surrounding plasma, apparently contradicting one of the bubble model's predictions. Nevertheless, it must be pointed out that even though pressure can be slightly larger than that of its neighbors, S could be still be smaller because the more dipolar field line configuration results in a smaller flux tube volume [see for example Wing et al., [2007] in regard to the substorm dipolarization]. Erickson [1992], however, raises another issue namely that substorm is preceded by growth phase and hence Pontius-Wolf bubbles are not sufficient to remove the catastrophic consequences of the pressure balance inconsistence at all times.

In the same paper that introduces pressure balance inconsistency, Erickson and Wolf [1980] suggests that a substorm can reduce S. Our result shows that substorm certainly reduces S significantly. However, the result here suggests that there is a substantial difference between the S reduction during the steady steady convection, e.g., growth phase, than during the transition from growth to expansion phases, i.e. before and after onset. The S reduction by a

factor of 1.5 during the growth phase is considerably smaller than S reduction by a factor of 8 after the substorm onset.

Other studies suggest that the pressure reduction can be achieved through reconnection [e.g., Borovsky et al., 1998; Nagai et al., 1998], resulting in the losses of the detached flux tubes and particles in the plasmoids and hence S. Kaufmann et al. [2004] considers this mechanism and claims that there is a scarcity of reconnection evidence earthward of X = -15 Re in the Geotail dataset created for all conditions, which makes it hard to explain the loss of S earthward of this location. Although their study rules out direct reconnection, it cannot rule out the possibility of reconnection tailward of X ~ -20 Re that leads to the bubble or plasmoid formation, which in turn leads to the losses of S. However, our result here suggests that S reduction from reconnection should be much larger (an order of magnitude) than S reduction during quasi-steady state (a factor of ~1.5).

After the onset and reconnection, it is not clear if the closed field line (left of the reconnection point in Figure 5b) would convect earthward adiabatically or non-adiabatically, e.g., if Pontius-Wolf bubbles would form and then convect earthward. S would be conserved in the former but S would decrease in the latter. Our expansion phase S profile, Figure 2f, shows that earthward of X = -20 Re, S decreases with decreasing distance in the X direction, suggesting that after reconnection, the flux tube loses S as it convects earthward. However, caution should be taken with this result during the expansion phase because statistical averaging of S on field lines that reconnect later in the expansion will overestimate S. The amount of overestimate would generally increase tailward---therefore the decrease of S earthward of 20. However, results may be believable earthward of the onset location. Our method and observations also cannot reveal if Pontius-Wolf bubbles actually form and/or if S is reduced by other mechanism(s).

Ion precipitation and auroral processes can also be the source of S reduction. However, the precipitation loss times are in the order of hours even for strong pitch angle scattering [Kennel, 1969]. Furthermore, Borovsky et al. [1998b] estimates that only about 10% of the ions of the plasma sheet are eventually lost to the atmosphere. As will be discussed later, this is much smaller than the 70% - 80% loss found in the flux tube from X = -30 Re to X = -10 Re.

Other studies suggest that this reduction in S during steady convection may be related to flux across field lines, e.g., ion gradient and curvature duskward drifts, that may also be related to the buildup in the pressure gradient, resulting in entropy loading of the duskside [e.g., Tsyganenko, 1982; Kivelson and Spence,1988; *Lyons et al.*, 2003b]. Ion duskward drift, which has been observed in several observational studies [e.g., Wang et al., 2006; 2007; Angelopoulos et al., 1993; Paterson et al., 1998; Hori et al., 2000] can lead to higher temperatures on the duskside at the inner plasma sheet and at geosynchronous orbit because of the drift temperature dependence [e.g., Korth et al., 1999; Wing and Newell, 1998; 2002; 2007]. Moreover, the duskward curvature and gradient drift of ions, which carry ~85% of the pressure [e.g., Baumjohann et al., 1989; Spence et al., 1989]), should carry a dawn to dusk heat flux in the entropy profiles. Indeed, this can be seen in the near earth region of the specific entropy (s) profiles shown in Figure 2a. In fact, dawn-dusk heat flux is seen in the substorm profiles for all substorm profiles in Figure 2 panels a – d, suggesting that gradient/curvature drift plays a significant role before and after the onset. Modeling works have shown that curvature and gradient drift is adequate to resolve the pressure balance inconsistency [e.g., Kivelson and Spence, 1988, Wang et al., 2001]. Nonetheless, other studies suggest that curvature and gradient drift may not be sufficient and that cross-tail diffusive and ExB drifts may also play significant roles [e.g., Angelopoulos et al., 2002; Ashour-Abdalla et al., 1998; Hori et al., 2000; Kaufmann et al., 2001; Erickson, 1992]. The latter relies on an earthward component of E, which would

lead to drifts in the Y or Z direction. However, the signature of cross-tail ExB or isothermic diffusive drifts would not be readily detected in the s profile such as the one shown in Figure 2a. Interestingly, in contrast to s profile, S profile does not exhibit noticeable dawn-dusk heat flux as can be seen in Figure 2e. The absence of strong dawn-dusk heat flux can also be found in previous studies using in situ measurements [e.g., Garner et al., 2003; Kaufman et al., 2004]. The main feature in the S profile in Figure 2e and in other S profiles is the radial reduction in S. The lack of dawn-dusk feature perhaps suggests that the reduction in V and/or equivalently the content of the flux tube volume, N, play a more significant role in determining the overall S contour. In principle, this difference in S and s also probably suggests that curvature and gradient drifts may not be sufficient to explain the loss of S. In particular, one might expect to at least see an azimuthal gradient in S.

If curvature/gradient, cross-tail ExB, and/or cross-tail diffusive drifts play significant role(s) in entropy reduction during earthward convection, then it would be expected that the total content of the flux tube, N, would also be significantly reduced. In the MHD approximation, N is proportional to S and therefore the loss of S could be interpreted as a loss of N (particularly in a region where s is conserved). However, in the case where s is not conserved across field lines, the constant of proportionality changes across field lines and the relative entropy loss may be somewhat different from the total particle content of a flux tube. Kaufman et al. [2004] finds that stastically in Geotail data, from X = -30 Re to X = -10 Re N is reduced by a factor of 70% while S is reduced 80 – 85%. Garner et al. [2003] finds N is reduced by a factor of 4 or about 75% from X = -27.7 Re to X = -11.5 Re. However, Borovsky et al. [1998b] finds the loss is smaller, about 30% but for X = -20 Re to X = -14 Re. In our data, during the growth phase, near the midnight meridian, from X = -30 Re to X = -10 Re, N is reduced by 70%, which is similar to the results reported by Kaufman et al. [2004] and Garner et al. [2003]. However, what is

interesting here is that most of the losses occur closer to Earth. From X = -30 Re to X = -20 Re, N is reduced only by ~20%, leaving 50% reduction between X = -20 Re to X = -10 Re. This strongly suggests that curvature and gradient drift, which becomes more dominant closer to Earth, at least partly, can play a role in the N and hence S reduction. In the recovery phase, the gradient in S is mostly in the –x direction at far distances down the tail, but the gradient becomes more radial closer to the earth suggestive that much plasma is carried azimuthally around the earth by curvature and gradient drift and cannot access the near earth region.

Due to their high speeds, and in frequent cases lower temperature (in the case of blobs; herein bubles refer to both bubbles and blobs) [e.g., Nakamura et al., 2001a; Sergeev et al., 1996; Kauffman and Paterson, 2006], it is expected that ***ExB*** convection would play a more significant role than curvature and gradient drift in the transport of the bubbles. Thus, the suggestion that curvature and gradient drift leads to the pressure reduction at the inner edge of the plasma sheet may be less of a factor. Hence, the low temperature bubbles (blobs) provide an ideal setting for testing this scenario, which will be investigated in a future study.

Unlike the total entropy, the specific entropy, $s = p/\rho^{\gamma}$, is an intensive variable of the system and should not depend on the system size. Specific entropy, has been reported to be nearly conserved in the plasma sheet during quiet or average magnetic conditions [Huang et al., 1989; Baumjohann, 1993; Goertz and Baumjohann, 1991]. This average property can be seen in Figure 6, which shows that distant tail, mid-tail, and near Earth plasma sheet have nearly similar adiabats (lie on the same line in Figure 6), albeit with noticeable scatter [Borovsky, GEM presentation, 2005]. Similar large scatter can also be observed in Baumjohann [1993] study. These large scatters can partly account for the observations that S is not exactly proportional to N, as discussed earlier. Some of these scatter may be due to the particles having a wide range of energies that curvature and gradient drift in and out of flux tube, violating the frozen in

assumption. The extent of the s conservation violation during the substorm growth phase can be seen in Figure 2a. There are several items of interest in this figure. First, it does appear that there are low entropy populations along the flanks, which appear to be related to lower temperature populations with higher density. The entropy appears to be about the same along the flank. They could have a source at the magentopause (perhaps akin to the cold, dense plasma sheet) or the tail where they convect earthward, but it remains an open question whether it is the remnant of cold, dense plasma from sustained northward IMF conditions or a population that enters during the growth phase. In any case, the entropy appears to vary only slightly along the X direction consistent also with earthward convection in a dawn-dusk electric field. Because the population is cold, it would be expected that curvature and gradient drifts are not as important. In the center of the plasma sheet is a high entropy population dominated by hot particles. As expected, the isoentropy contours for that population has a significant duskward component consistent with curvature and gradient drift. On the other hand, Figure 4 panels a – c, which examine se/sg, ser/sg, and slr/sg respectively, suggest that s appears to be approximately or roughly (not exactly) conserved through out the substorm phases. This result would be consistent with S or volume or mass reduction during the onset without significant plasma heating or heat flux, e.g., plasmoid.

Another view of substorm expansion is that it occurs when field lines diffuse through a turbulent region. In this case, the particles/fluid are not frozen to the field lines and a decrease in entropy may be expected as the flux tube volume decreases and plasma is lost. However, it is uncertain whether the specific entropy would be conserved through such particle transport. Estimating how S would change for various candidate transport models, and whether specific entropy would remain relatively invariant compared with the significant loss of S, would be useful.

6. Summary and conclusion

The entropy properties of the plasma sheet during substorm are investigated during (a) quasi-steady state and (b) phase transitions.

<u>Quasi-steady state entropy profiles</u>

- The total entropy, S, increases with increasing radial distance from the Earth, a phenomenon commonly known as pressure balance inconsistentency. The loss of S is accompanied by a huge loss of the flux tube content, N. The loss of N increases more rapidly closer to Earth, which suggests that curvature and gradient drift can, at least partly, play a role in the reduction of N and hence S.
- The specific entropy, s, is conserved in the X direction or convection direction.
- There is a dawn-dusk asymmetry in s profile in the near-Earth region that is consistent with the duskward heat flux carried by the curvature/gradient drift.
- In the early and late recovery phases, s has a minimum at postmidnight that is associated with cold dense ions, which may be associated with ion outflow.

<u>Substorm transition phase entropy profiles</u>

- After substorm onset, earthward of 20 Re, $|Y| < 10$ Re, S is reduced by an order of magnitude. The loss of S is consistent with Birn et al. [2006a] simulation, which suggests that after reconnection, the flux tube volume and its contents are lost to the plasmoid ejected tailward of the X line. The order of magnitude S reduction is significantly higher than S reduction (a factor ~ 1.5) during the quasi-steady state, e.g., growth phase.

- In contrast, s does not change much before and after substorm onset, which suggests that reconnection only affects the plasma in a small dissipation region, leaving much of the plasma in the flux tube unchanged. Hence, s and S of the entire closed system that includes the plasmoid should be approximately conserved. However, as far as S is concerned, if one were to consider only the closed field line, reconnection does change the field line connectivity and topology, which can significantly reduce S on the field line that is still attached to the Earth (the closed field line).

Acknowledgments. Gordon Wilson has been helpful in our acquiring DMSP SSJ4 data, as has the World Data Center in Boulder, Colorado. Simon Wing thanks Michelle Thomsen for helpful discussions. Simon Wing gratefully acknowledges support from NSF Grants ATM-0703445, ATM-0802715, and ATM-0538513; and NASA Grant NNX06AB87G. Jay R. Johnson acknowledges support from NASA grants (NNH04AB23I, NNH04AA73I, NNG06GE96G, NNX06AB87G and NNH07AF37I), and NSF grants (ATM0411392 and ATM0614012, add our NSF grant), and DOE contract DE-AC02-76CH03073.

References

Angelopoulos, V., W. Baumjohann, C. F. Kennel, F. V. Coroniti, M. G. Kivelson, R. Pellat, R. J. Walker, H. Lu¨hr, and G. Paschmann (1992), Bursty bulk flows in the inner central plasma sheet, J. Geophys. Res., 97,4027–4039.

Angelopoulos, V., et al. (1993), Characteristics of ion flow in the quiet state of the inner plasma sheet, Geophys. Res. Lett., 20, 1711 – 1714.

Ashour-Abdalla, M., et al. (1998), Determination of particle sources for a Geotail distribution function observed on May 23, 1995, in Geospace Mass and Energy Flow, edited by J. L. Horwitz et al., pp. 297– 312, AGU, Washington, D.C.

Bernstein, W., B. Hultqvist, and H. Borg (1974), Some implications of low altitude observations of isotropic precipitation of ring current protons beyond the plasmapause, *Planet. Space Sci*., 22, 767.

Baumjohann, W., and G. Paschmann (1989), Determination of the polytropic index in the plasma sheet, Geophys. Res. Lett., 16, 295– 298.

Baumjohann, W., R. Schodel, and R. Nakamura, Bursts of fast magnetotail flux transport (2002), Adv. Space. Sci., 30, 2241-2246.

Baumjohann, W., G. Paschmann, and C. A. Cattell (1989), Average plasma properties in the central plasma sheet, *J. Geophys. Res*., *94*, 6597–6606.

Baumjohann, W., The near-Earth plasma sheet: An AMPTE?IRM perspective (1993), Spa Sci Rev, 64, 141-163, 1993.

Birn J., M. Hesse, and K. Schindler (2006a), On the role of entropy conservation and entropy loss governing substorm phases, Int. Conf. Substorms-8, 19-24.

Birn, J., M. Hesse, and K. Schindler, Entropy conservation in simulations of magnetic reconnection (2006b), Phys. Of Plasma, 13, 092117, doi: 10.1063/1.2349440.

Borovsky, J. E., M. F. Thomsen, and R. C. Elphic (1998), The driving of the plasma sheet by the solar wind, J. Geophys. Res., 103, 17,617–17,639.

Borovsky, J. E., M. F. Thomsen, R. C. Elphic, T. E. Cayton, and D. J. McComas (1998b), The transport of plasma sheet material from the distant tail to geosynchronous orbit, J. Geophys. Res., 103, A9, 20,297-20,331.

Chen, C. X., and R. A. Wolf (1993), Interpretation of high-speed flows in the plasma sheet, J. Geophys. Res., 98, 21,409-21,419.

Erickson, G. M., and R. A. Wolf (1980), Is steady convection possible in the Earth's magnetotail, Geophys. Res. Lett., 7, 897.

Erickson, G. M. (1992), A quasi-static magnetospheric convection model in two dimensions, J. Geophys. Res., 97, 6505-6522.

Friedel, R. H. W., H. Korth, M. G. Henderson, and M. F. Thomsen (2001), Plasma sheet access to the inner magnetosphere, *J. Geophys. Res*., *106*, 5845-5858.

Fujimoto, M., T. Terasawa, T. Mukai, Y. Saito, T. Yamamoto, and S. Kokubun (1998), Plasma entry from the flanks of the near-Earth magnetotail: Geotail observations, *J. Geophys. Res*., *103*, 4391-4408.

Garner, T. W., R. A. Wolf, R. W. Spiro, M. F. Thomsen, and H. Korth (2003), Pressure balance inconsistency exhibited in a statistical model of magnetospheric plasma, J. Geophys. Res., 108(A8), 1331, doi:10.1029/2003JA009877.

Gjerloev, J. W., R. A. Hoffman, J. B. Sigwarth, L. A. Frank (2007), Statistical description of the bulge-type auroral substorm in the far ultraviolet, *J.Geophys.Res*., in press.

Goertz, C. K., and W. Baumjohann (1991), On the thermodynamics of the plasma sheet, *J. Geophys. Res.*, *96*, 20,991-20,998.

Gombosi, T. I., and A. F. Nagy (1989), Time-dependent modeling of field-aligned current-generated ion transients in the polar wind, *J. Geophys. Res*., *94*, 359-369.

Hori, T., K. Maezawa, Y. Saito, and T. Mukai (2000), Average profile of ion flow and convection electric field in near-Earth plasma sheet, Geophys. Res. Lett., 27, 1623–1626.

Huang, C. Y., and L. A. Frank (1994), A statistical survey of the central plasma sheet, *J. Geophys. Res*., 99, 83-95.

Huang, C. Y., C. K. Goertz, L. A. Frank, and G. Rostoker (1989), Observational determination of the adiabatic index in the quiet time plasma sheet, Geophys. Res. Lett., 16, 563– 566.

Kamide, Y., and S. Kokubun (1996), Two-component auroral electrojet: Importance for substorm studies, *J.Geophys.Res*., *101*, 13.027.

Kaufmann, R. L., W. R. Paterson, and L. A. Frank (2004), Pressure, volume, density relationships in the plasma sheet, J. Geophys. Res., 109, A08204, doi:10.1029/2003JA010317.

Kaufmann, R. L., and W. R. Paterson 2006), Magnetic flux and particle transport in the plasma sheet, J. Geophys. Res., 111, A10214, doi:10.1029/2006JA011734.

Kennel, C. F. (1969), Consequences of a mangetospheric plasma, Rev. Geophys., 7, 379.

Kistler, L. M., E. Mobius, W. Baumjohann, G. Paschmann, and D. C. Hamilton (1992), Pressure changes in the plasma sheet during substorm injections, *J. Geophys. Res*., *97*, 2973-2983.

Kivelson, M. G., and H. E. Spence (1988), On the possibility of quasistatic convection in the quiet magnetotail, Geophys. Res., Lett., 15, 1541-1544.

Korth, H., M. F. Thomsen, J. E. Borovsky, and D. J. McComas (1999), Plasma sheet access to geosynchronous orbit, *J. Geophys. Res., 104*, 25,047-25,061.

Lui, A. T. Y. (1991), Extended consideration of a synthesis model for magnetospheric substorms, in *Magnetospheric Substorms*, pp. 43-60, *Geophys. Monog.*, *64*, edited by J. R. Kan, T. A. Potemra, S. Kokubun, and T. Ijima, AGU, Washington D.C.,

Lyons, L. R., and T. W. Speiser (1982), Evidence for current sheet acceleration in the geomagnetic tail, J. Geophys. Res., 87, 2276-2286.

Lyons, L. R., C.-P. Wang, T. Nagai, T. Mukai, Y. Saito, and J. C. Samson (2003a), Substorm inner plasma sheet particle reduction, *J. Geophys. Res*., 108(A12), 1426, doi:10.1029/2003JA010177.

Lyons, L. R., C.-P. Wang, and T. Nagai (2003b), Substorm onset by plasma sheet divergence, *J. Geophys. Res*., 108(A12), 1427, doi:10.1029/2003JA010178.

McPherron, R. L., C. T. Russell, and M. P. Aubry (1973), Satellite studies of magnetospheric substorms on August 15, 1968, 9, Phenomenological model for substorms, *J. Geophys. Res*., 78, 3131.

Nagai, T., M. Fujimoto, Y. Saito, S. Machida, T. Terasawa, R. Nakamura, T. Yamamoto, T. Mukai, A. Nishida, and S. kokubun (1998), Structure and dynamics if nagnetic reconnection for substorm onsets with Geotail observations, J. Geophys. Res., 103, 4419-4440.

Opgenoorth, H. J., M. A. L. Persson, T. I. Pulkkinen, and R. J. Pellinen (1994), Recovery phase of magnetospheric substorms and its association with morning-sector aurora, *J. Geophys. Res*., *99*, 4115-4129.

Paterson, W. R., L. A. Frank, S. Kokubun, and T. Yamamoto (1998), Geotail survey of ion flow in the plasma sheet: Observations between 10 and 50 RE, J. Geophys. Res., 103, 11,811 – 11,825.

Pontius, D. H., and R. A. Wolf (1990), Transient flux tubes in the terrestrial magnetosphere, Geophys. Res. Lett., 17, 49-52.

Pulkkinen, T. I., and N. A. Tsyganenko (1996), Testing the accuracy of magnetospheric model field line mapping, *J. Geophys. Res., 101*, 27,431-27,442.

Sergeev, V. A., M. Malikov, and K. Mursula (1993), Testing the isotropic boundary algorithm method to evaluate the magnetic field configuration in the tail, *J. Geophys. Res*., 98, 7609-7620.

Sergeev, V. A., V. Angelopoulos, J. T. Gosling, C. A. Cattell, and C. T. Russell (1996), Detection of localized, plasma-depleted flux tubes or bubbles in the midtail plasma sheet, J. Geophys. Res., 101, 10,817– 10,826.

Spence, H. E., and M. G. Kivelson (1993), Contributions of the low-latitude boundary layer to the finite width magnetotail convection model, *J. Geophys. Res*., *98*, 15,487-15,496.

Spence, H. E., M. G. Kivelson, R. J. Walker, and D. J. McComas (1989), Magnetospheric plasma pressures in the midnight meridian: Observations from 2.5 to 35 *RE*, *J. Geophys. Res.*, *94*, 5264–5272.

Terasawa, T. et al. (1997), Solar wind control of density and temperature in the near-Earth plasma sheet: WIND/GEOTAIL collaboration, *Geophys. Res. Lett*., *24*, 935-938.

Tsyganenko, N. A. (1982), On the convective mechanism for formation of the plasma sheet in the magnetospheric tail, Planet Space Sci., 30, 1007-1012.

Tsyganenko, N. A. (1989), A magnetospheric magnetic field model with a warped tail current sheet, *Planet Space Sci*., *37*, 5-20.

Tung, Y.-K., C. W. Carlson, J. P. McFadden, D. M. Klumpar, G. K. Parks, W. J. Peria, and K. Liou (2001), Auroral polar cap boundary ion conic outflow observed on FAST, J. Geophys. Res., 106, 3603-3614.

Usadi, A., R. A. Wolf, M. Heinemann, and W. Horton (1996), Does chaos alter the ensemble averaged drift equation?, J. Geophys. Res., 101, 15,491.

Wang, C. P., L. R. Lyons, M. W. Chen, and R. A. Wolf (2001), Modeling the quiet time inner plasma sheet protons, J. Geophys. Res., 106, 6161.

Wang, C.-P., L. R. Lyons, M. W. Chen, and F. R. Toffoletto (2004), Modeling the transition of the inner plasma sheet from weak to enchanced convection, *J. Geophys. Res., 109*, A12202, doi:10.1029/2004JA010591.

Wang, C.-P., L. R. Lyons, J. M. Weygand, T. Nagai, and R. W. McEntire (2006), Equatorial distributions of the plasma sheet ions, their electric and magnetic fields under different interplanetary magnetic field Bz conditions, J. Geophys. Res., 111, A04215, doi:10.1029/2005JA011545.

Wang, C.-P., L. R. Lyons, T. Nagai, J. M. Weygand, and R. W. McEntire (2007), Sources, transport, and distributions of plasma sheet ions and electrons and dependence on interplanetary parameters under northward interplanetary magnetic field, J. Geophys. Res., 112, A10224, doi:10.1029/2007JA012522.

Wilson, G. R., D. M. Ober, G. A. germany, and E. J. Lund (2004), Nightside auroral zone and polar cap ion outflow as a function of substorm size and phase, *J. Geophys. Res*., *109*, A02206, doi:10.1029/2003JA009835.

Wing, S., and P. T. Newell (1998), Central plasma sheet ion properties as inferred from ionospheric observations, *J. Geophys. Res*., *103*, 6785-6800.

Wing, S., and P. T. Newell (2000), Quiet time plasma sheet ion pressure contribution to Birkeland currents, *J. Geophys. Res*., *105*, 7793-7802.

Wing, S., D. G. Sibeck, M. Wiltberger, and H. Singer (2002), Geosynchronous magnetic field temporal response to the solar wind and IMF variations, *J. Geophys. Res*., 107(A8), doi:10.1029/2001JA009156.

Wing, S., and Patrick T. Newell (2002), 2D plasma sheet density profile for northward and southward IMF, *Geophys. Res. Lett*., 29(9), 10.1029/2001GL013950.

Wing, S., J. R. Johnson, P. T. Newell, and C.-I. Meng (2005), Dawn-dusk asymmetry in the northward IMF plasma sheet, *J. Geophys. Res*., *110*, A08205, doi:10.1029/2005JA011086.

Wing, S., J. W. Gjerloev, J. R. Johnson, and R. A. Hoffman (2007), Substorm plasma sheet ion pressure profiles, *Geophys. Res. Lett*., 34, L16110, doi:10.1029/2007GL030453.

Winglee, R. M., W. Lewis, and G. Lu (2005), Mapping of the heavy ion outflows as seen by IMAGE and multifluid global modeling for the 17 April 2002 storm, *J. Geophys. Res.*, *110*, A12S24, doi:10.1029/2004JA010909.

Wolf, R. A., V. Kumar, F. R. Toffoletto, G. M. Erickson, A. M. Savoie, C. X. Chen, and C. L. Lemon (2006), Estimating local plasma sheet $PV^{5/3}$ from single-spacecraft measurements, *J. Geophys. Res*., *111*, A12218, doi:10.1029/2006JA012010.

Wolf, R. A. (1983), The quasi-static (slow-flow) region of the magnetosphere, in Solar-Terrestrial Physics, edited by R. L. Carovillano and J. M. Forbes, p. 303, D. Reidel, Hingham, Mass, 1983.

Table

substorm phase	location (X,Y,Z) R_E	flux tube volume	ion pressure (nPa)	S = $p^{1/\gamma}$ V	density (cm^{-3})	s = p/n^{γ}
midtail:						
growth	A = (–30,0,0)	8724	0.31	4320	0.49	1.0
expansion	C = (–20,0,0)	7899	0.55	5518	0.83	0.75
near-Earth:						
growth	A = (–20,0,0)	3976	0.53	2717	0.89	0.65
expansion	C = (–7,0,0)	379	0.90	356	1.2	0.66

Table 1. Flux tube volumes, ion pressure, density, entropy, and specific entropy (p/n^{γ}) for growth and expansion phases in the midnight meridian. Pressures and densities from Figure 2 are averaged in 6 × 6 R_E bin. See the schematic for the magnetic field line configurations in Figure 3.

Figure Caption

Figure 1. An example substorm occurring on October 23, 1997. Top panels show VIS Earth Camera images (124–149 nm) obtained during the four substorm phases with DMSP passes superposed. Noon is at the top and midnight at the bottom. Bottom panels show the equatorial pressure inferred from the measured DMSP particle precipitation observations.

Figure 2. Panels (a–d) average equatorial pressure profiles inferred from all DMSP observations during growth, expansion, early recovery, and late recovery phases, respectively, and their corresponding (e – h) density and (i – l) temperature profiles.

Figure 3. Schematics depicting the field line configurations for growth and expansion phases. See text for full explanations.

Figure 4. Comparisons of equatorial plane s and S profiles from expansion; early and late recovery phases to those from growth phase. Panels (a – c) and (d – f) are for specific entropies and total entropies, respectively. The subscript g = growth phase, e = expansion phase, er = early recovery phase, and lr = late recovery phase.

Figure 5. Evolutions of MHD simulation magnetic field lines and their entropies during substorm phases (from Figures 2 an 3 in Birn et al. [2006a]). Panel (a) shows the evolution of magnetic field lines (denoted by constant value of vector potential A) while panel (b) shows the evolution of the entropy as a function of field line. We consider the evolution of a particular

field line shown in red in panel (a) with a value of A indicated by the dashed red line in panel (b). The simulation begins from a stretched magnetotail configuration. As the simulation proceeds a thin current sheet forms leading to reconnection. Initially field lines at smaller value of A (than the red line) reconnect and the red field line stretches around the ejected plasmoid material (t=50). Eventually, the red field line reconnects and develops two flux systems---one connected to the left boundary of the simulation and the other as part of the plasmoid. As the simulation proceeds the entropy first slightly increases (because the field line stretches around the plasmoid) and then following reconnection the entropy drops to a constant value for the remainder of the simulation. The entropy here is computed only for the part of the flux system connected to the left boundary and does not include the plasmoid entropy. It should be noted that all subsequent field lines that reconnect drop to the same value of entropy.

Figure 6. Entropy density of plasma sheet, LLBL, and magnetosheath ions in the n – T semi log space. The ions in the distant, mid-tail, and near-Earth plasma sheet tend to have the same adiabats, indicated by the diagonal lines with $\gamma = 5/3$ (from Joseph Borovsky, GEM presentation 2005).

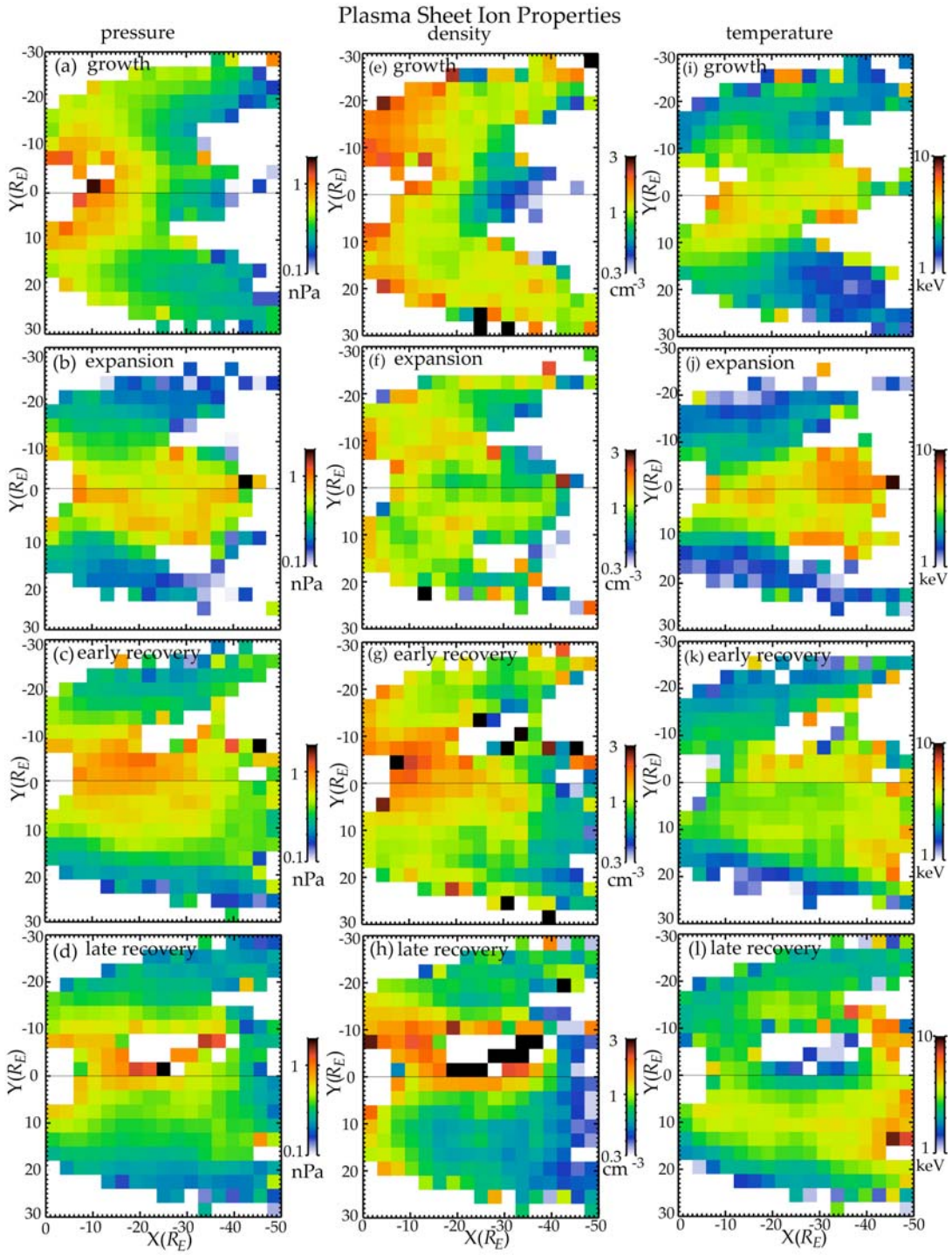
Plasma Sheet Ion Properties
pressure
density
temperature
(a) growth
(b) expansion
(c) early recovery
(d) late recovery
(e) growth
(f) expansion
(g) early recovery
(h) late recovery
(i) growth
(j) expansion
(k) early recovery
(l) late recovery
nPa
cm^{-3}
keV
Y(R_E)
X(R_E)

Figure 1.

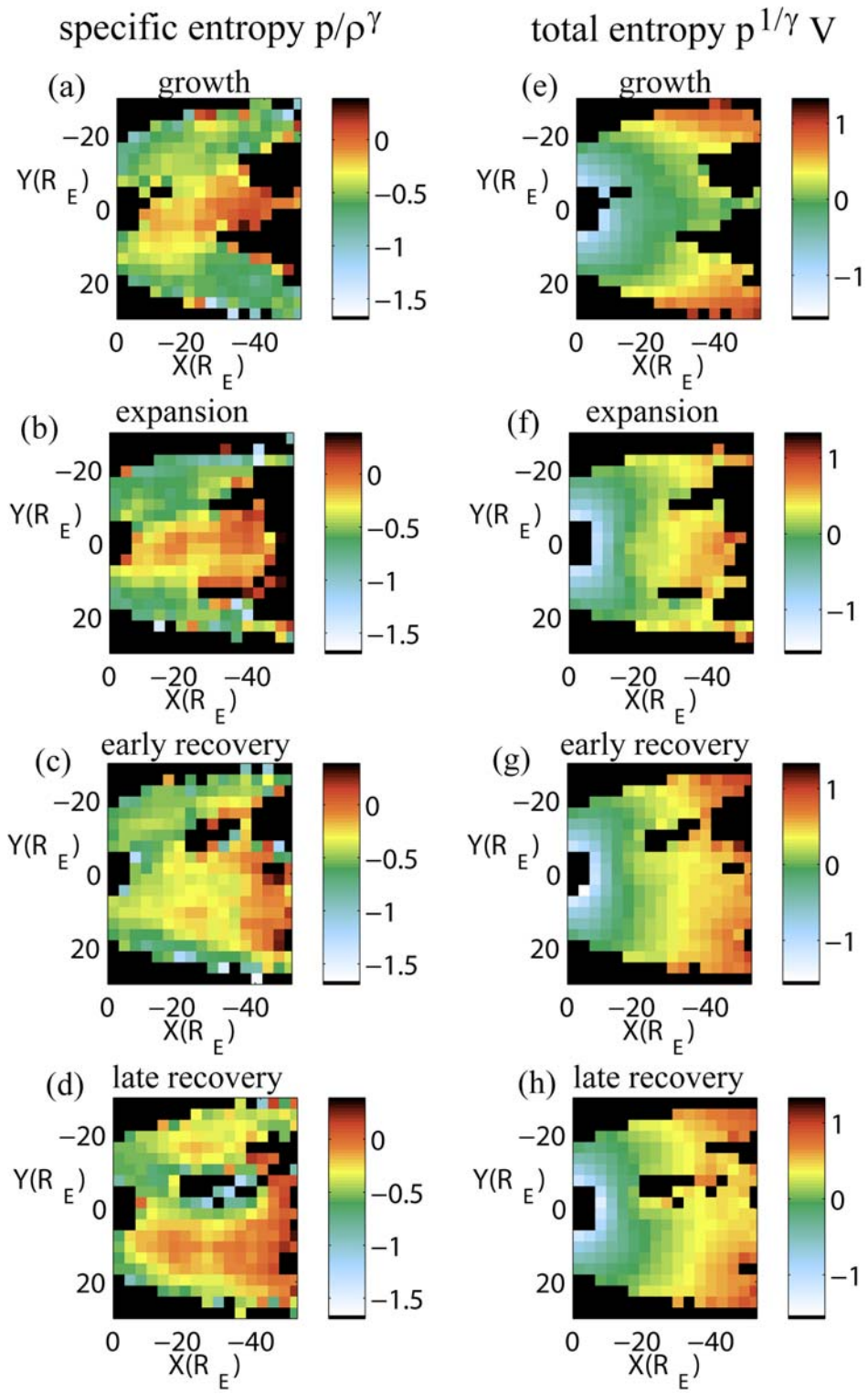
specific entropy p/ρ^γ
total entropy p^1/γ V
(a) growth
(b) expansion
(c) early recovery
(d) late recovery
(e) growth
(f) expansion
(g) early recovery
(h) late recovery
Y(R E)
X(R E)
−20
0
20
0
−20
−40
0
−0.5
−1
−1.5
1
0
−1

Figure 2

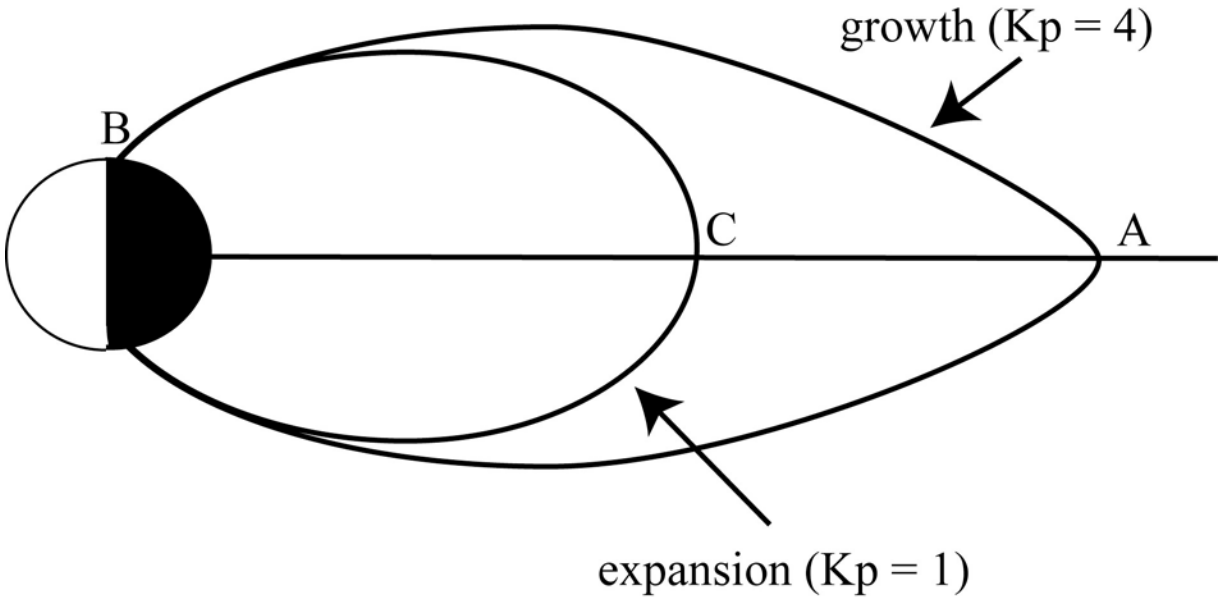

Figure 3

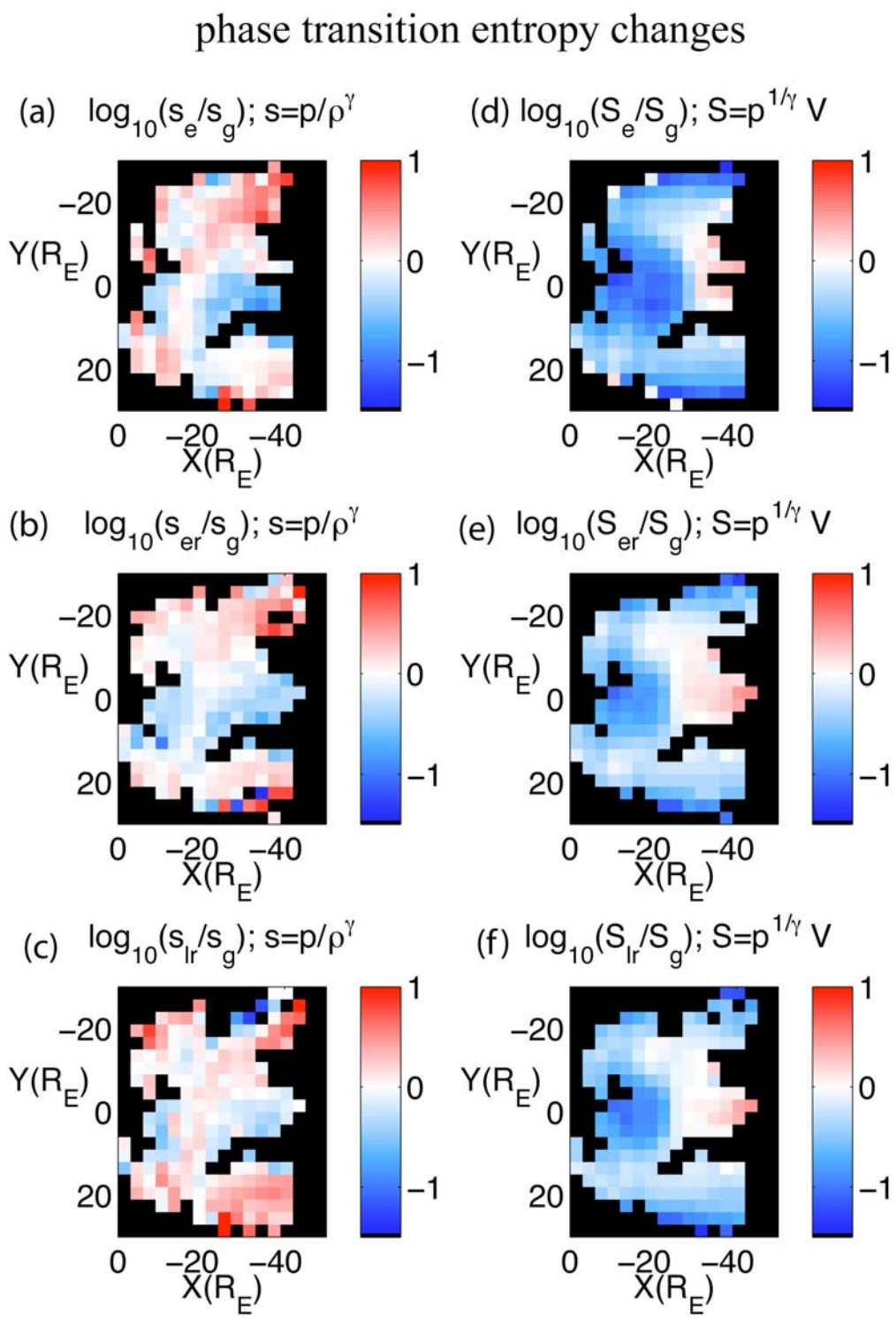
phase transition entropy changes
(a) log10(se/sg); s=p/ργ
(d) log10(Se/Sg); S=p1/γ V
(b) log10(ser/sg); s=p/ργ
(e) log10(Ser/Sg); S=p1/γ V
(c) log10(slr/sg); s=p/ργ
(f) log10(Slr/Sg); S=p1/γ V
Y(RE)
X(RE)
−20
0
20
−40
1
0
−1

Figure 4.

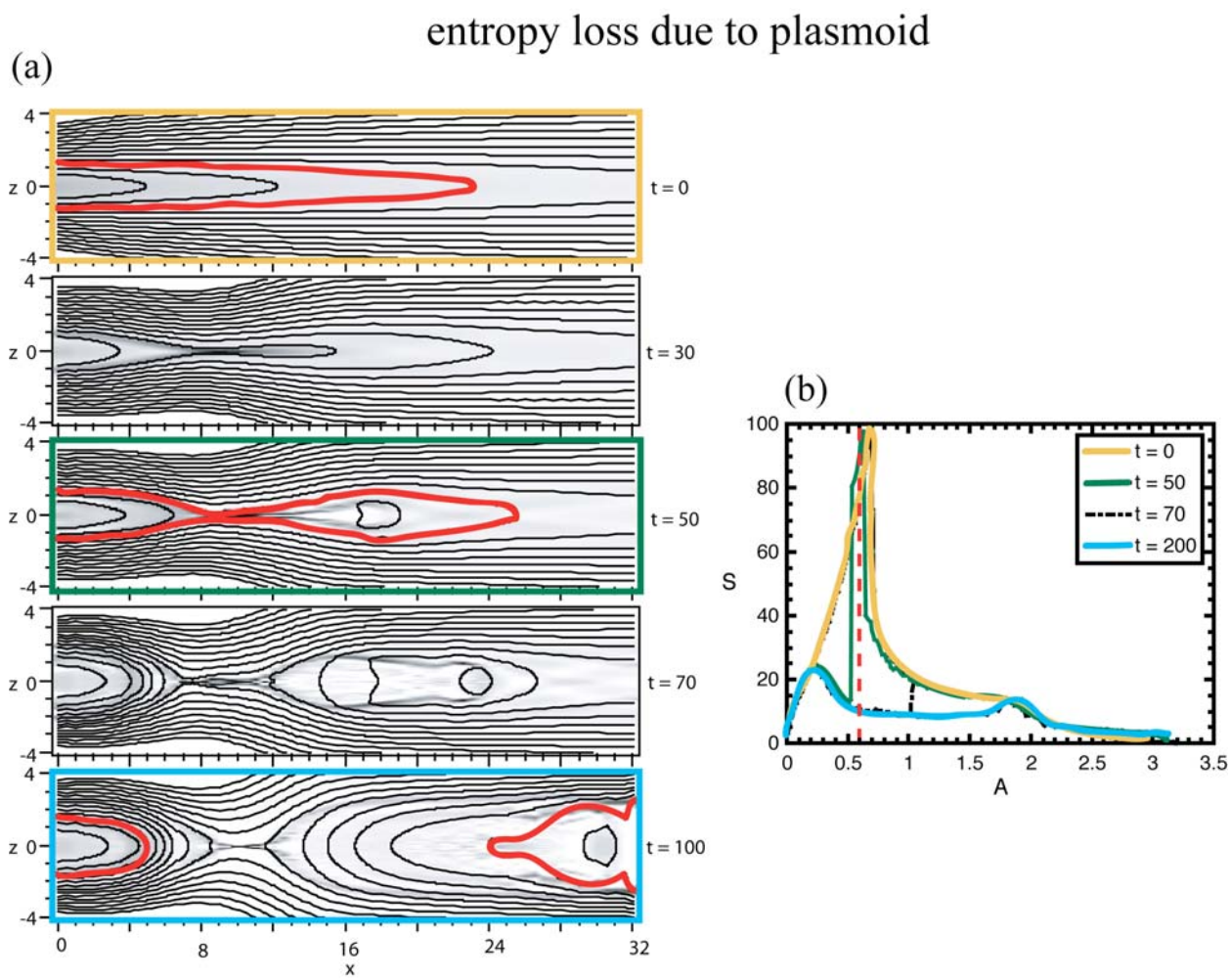
entropy loss due to plasmoid
(a)
t = 0
t = 30
t = 50
t = 70
t = 100
z
x
(b)
t = 0
t = 50
t = 70
t = 200
S
A

Figure 5

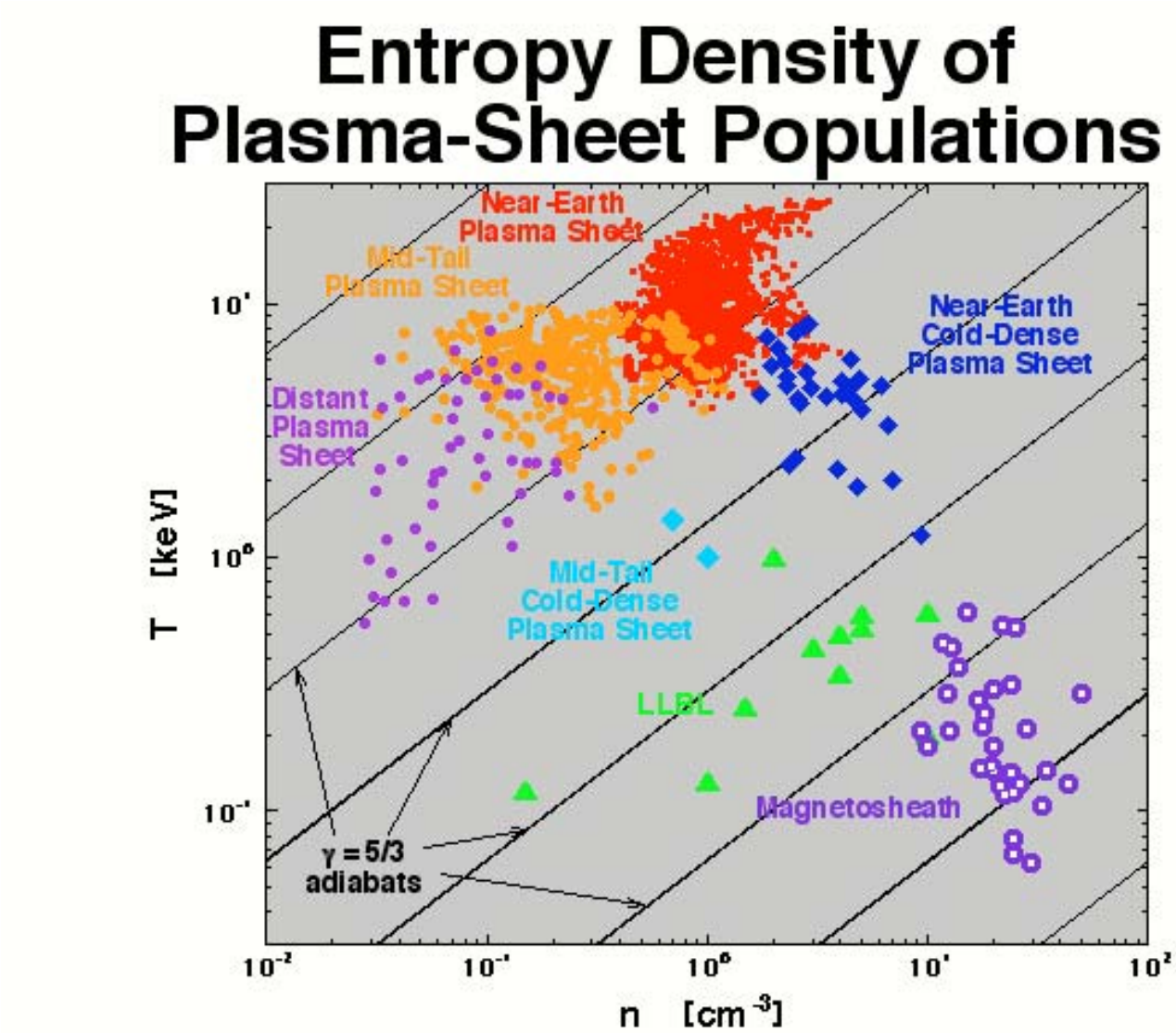
Entropy Density of
Plasma-Sheet Populations
Near-Earth
Plasma Sheet
Mid-Tail
Plasma Sheet
Near-Earth
Cold-Dense
Plasma Sheet
Distant
Plasma
Sheet
Mid-Tail
Cold-Dense
Plasma Sheet
LLBL
Magnetosheath
γ = 5/3
adiabats
T [keV]
n [cm⁻³]

Figure 6.